International Journal of Engineering and Advanced Technology (IJEAT)
ISSN: 2249-8958 (Online), Volume-2 Issue-6, August 2013

Numerical Modelling and Experimental Validation of a Vertical Spindle Model

Bindu Kumar Karthikeyan

Abstract - Numerical modelling of a vertical spindle is presented. Numerical model is assumed to have five degrees of freedom. The results obtained from the numerical modelling are used to verify with the spectra obtained from experiments. The experiments are done in a high speed high precision router spindle running at 25,000 rpm, employing high quality ceramic bearings. Fine measurement of spindle vibration characteristics is carried out using laser vibrometry. The comparison of the results shows close match. The validated model then provides contact loads which are used for elastohydrodynamic analysis of grease lubricated contacts

Index Terms: Precision high speed spindles, Numerical modelling of spindle, laser vibrometry

I. INTRODUCTION

The demand for higher productivity and improved quality of the machined surfaces requires spindle designers to aim for higher spindle speeds and feed rates. The high speed machine tool spindles used in routing operations require high dynamic stiffness to avoid vibration, which if not attained, can have dramatic damaging effects on surface finish, wheel wear, and form-holding. The spindle experimental spectra at high speeds will be a combination of various modulation effects, which makes it extremely difficult for the successful isolation and attribution of certain effects to specific causes even with latest diagnostic techniques. The need to develop a realistic bearing theoretical simulation model is of high importance since bearing systems are the major sources of vibration within the high speed precision machine spindles.

The first simulation model in this respect was from Rahnejat and Gohar [1] for a rigid rotor supported with a pair of deep groove ball bearings with two degrees of freedom. The natural frequency of a perfect spindle/bearing assembly was found to be dependent upon the spindle mass and the bearing stiffness and independent of rotational speed. Bearing stiffness was found to be depending upon the radial clearance and number of balls as observed by Wardle et.al [2]. Mastubara [3] modified this model by incorporating the modal response of the elastic shaft and effect of damping. Five degrees of freedom analysis of an asymmetrical spindle, supported by a pair of back-to-back angular contact ball bearings was devised by Aini et. al.[4] with applied axial and radial loads. The model was used [5] to simulate the vibration characteristics of a precision grinding spindle with metallic ball/raceways. Aini et al.[8] extended their five degree of freedom model by including the squeeze film effect caused by the mutual convergence of bearing rings.

Manuscript published on 30 August 2013.
***** Correspondence Author (s)
Bindu Kumar Karthikeyan, Government Engineering College, Thiruvananthapuram, Kerala, India

The overall system response, when subjected to varying spindle mass or the number of balls in the support bearings was studied. The overall contribution to damping of the elastohydrodynamic oil films between the rolling elements and their raceways is shown to be slight.

All of the studies reported above are for horizontally mounted spindle units; these require no external sources of excitation owing to the partly loaded region of the bearing. The vibrations generated are known as 'variable-compliance vibrations' which has been reported in various references [2,12]. In case of a vertically mounted spindle units the non existence of loaded region reduces the vibration, but the inherent feature of the bearings distributing the loads through the rolling elements and periodic variation of stiffness generates vibration. Numerical analysis for the dynamics a perfect ball bearing in vertical spindle is presented with comparison of experimental spectra from a high speed high precision routing spindle. Contact loads obtained from the validated model are used for finding the behaviour of grease lubricated conjunctions without considering effect of squeeze.

II. PRECISION SPINDLE MODEL

For this mathematical modelling the spindle is considered to have five degrees of freedom motion. The five degrees of freedom are along axial Z, radial X and Y and the rocking modes ϕ and φ about the X and Y axes respectively. The schematic of spindle, showing the five degrees of freedom is shown in Figure 1.

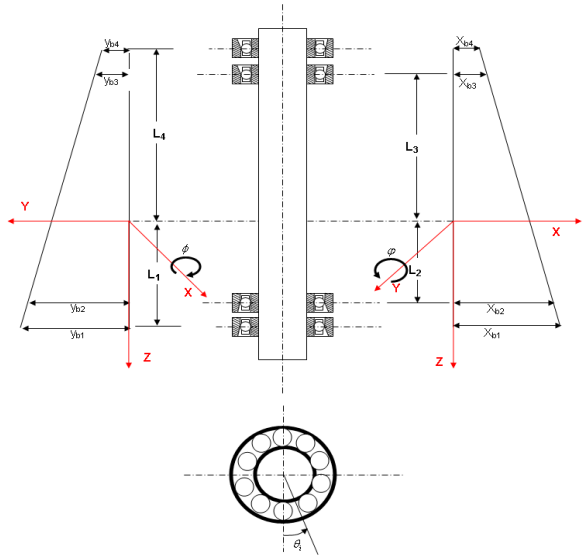

Figure. 1 Schematic representation of vertical spindle assembly

Published By:
Blue Eyes Intelligence Engineering and Sciences Publication (BEIESP)

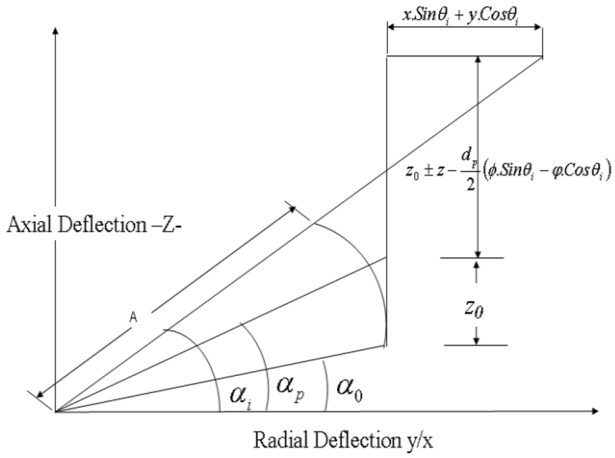

Figure.2 Displacement of raceway curvature centres.

The flexural natural modes of spindle are eliminated by considering it to be rigid. The balls are considered to be massless and equi-spaced around the inner ring. The centrifugal effects and torsional effects of the spindle are neglected. Sources of damping are excluded for the initial part, where dry Hertzian contacts are considered. Due to the elliptical elastostatic footprints of ball-to-races contacts, contact loads are obtained according to the classical Hertzian theory [9].

Figures 1 and 2 show the deflection of the ith ball in terms of x, y and z displacements of the centre of gravity of the rotor in the X,Y and Z directions, as well as the tilts ϕ and φ about the X and Y directions. The total deflection of the ith ball-raceway contact is given by:

$$\delta_i = \left\{ \left[A.Sin\alpha_0 + z_0 - z - \frac{d_p}{2}\left(\phi.Cos\theta_i + \varphi.Sin\theta_i\right) \right]^2 + \left[A.Cos\alpha_p + \delta_0.Cos\alpha_p + x_b.Cos\theta_i + y_b.Sin\theta_i \right]^2 \right\}^{\frac{1}{2}} - A \qquad (1)$$

and the resulting transient contact angle is given by:

$$\alpha_i = \left(\frac{A.Sin\alpha_0 + z_0 - z - \frac{d_p}{2}\left(\phi.Cos\theta_i + \varphi.Sin\theta_i\right)}{A.Cos\alpha_p + \delta_0.Cos\alpha_p + y.Cos\theta_i + x.Sin\theta_i} \right) \qquad (2)$$

III. EQUATIONS OF MOTION

Figure 1 is a schematic representation of the spindle assembly. The spindle has displacements in X,Y and Z directions and rocking/tilting motions in both the radial directions, which are the five degrees of freedom. Care has been taken during modelling to keep the model to be generic so that in future model can be used for any vertically mounted spindle in any application. Referring to figure 1 the equations of motion for this high speed precision spindle in all the five degrees of freedom are:

$$M\ddot{x} = \sum_{i=1}^{n} W_i Sin\alpha - F_x \qquad (3)$$

$$M\ddot{y} = \sum_{i-1}^{n} W_i Cos\alpha_i Sin\theta_i - F_y \qquad (4)$$

$$M\ddot{z} = \sum_{i=1}^{n} W_i Cos\alpha_i Cos\theta_i + Mg - F_z \qquad (5)$$

$$I_{xx} - I_{zz}\omega\dot{\phi} = \sum_{i=1}^{n} LW_i Cos\alpha_i Cos\theta_i + \frac{1}{2}\sum_{i=1}^{n} d_p W_i Sin\alpha_i Cos\theta_i + LF_y \qquad (6)$$

$$I_{yy} + I_{zz}\omega\dot{\phi} = \sum_{i=1}^{n} LW_i Cos\alpha_i Sin\theta_i + \frac{1}{2}\sum_{i=1}^{n} d_p W_i Sin\alpha_i Sin\theta_i + LF_x \qquad (7)$$

The governing equations of motion in this five degrees of freedom system are solved by an iterative marching procedure, incorporating a third order quasi-linear method known as the Newmark linear acceleration technique as explained in reference [11]

IV. EXPERIMENTAL SETUP

1) Spindle Design and monitoring considerations

The current study employs a newly developed precision routing spindle for high speed applications has a 7.5 kW power, which can hold cutters up to 7.5 Kg. In order to investigate its vibration characteristics, it is mounted on a cast iron pedestal which is in turn attached firmly to a heavy cast iron machine bed. Cast iron structures are used, because of their good damping characteristics, caused by their structural porosity. The large mass of the assembly, fixed rigidly to a concrete foundation, places its natural modal frequencies considerably above the frequencies of generated vibration due to any synchronous out-of-balance of tool-spindle assembly or induced by the support bearings. The purpose of study is to monitor spindle vibration and obtain real time power spectra under free running (i.e. no cutting action) condition with a specimen held in the chuck to represent a tool, which will be a true representation of the numerical model. Under the spindle free running condition, the system is subjected to a pre-determined axial preload and a suitable radial interference. Therefore, the main sources of vibration are due to the imperfections on rolling elements' and raceways' surfaces, as well as the bearings' variable compliance effect and any out-of-balance in the spindle-tool assembly. For minimising effect of the sources of vibration, the spindle is supported by pairs of angular contact ball bearings in a arrangements and in a back-to-back arrangement at each end of the spindle, providing the desired high dynamic stiffness The specifications of these bearings are given in Table 1.

Table 1 Specification of bearings

	Tool end bearing	***Free end bearing***
Ball diameter	4.762mm	3.969 mm
Number of balls	23	20
Preloaded contact angle	15^0	15^0
Pitch diameter	48.698mm	36.012 mm
Inner race diameter	43.726mm	32.022 mm
Outer race diameter	53.46mm	39.981 mm
Material of balls	Ceramic Alumina	Ceramic Alumina

Published By:
Blue Eyes Intelligence Engineering
and Sciences Publication (BEIESP)

2) Sensors and data acquisition system

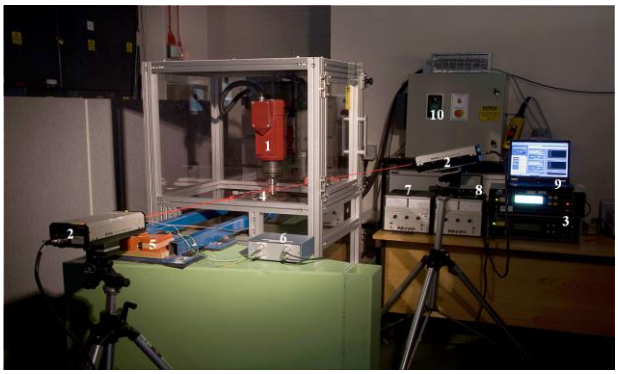

1 – High speed precision spindle
2 - Laser vibrometer
3 – Laser vibrometer controller
4 – Eddy Current probes
5 – Eddy Current driver
6 – Eddy Current band-pass filter
7 – PSU's
8 – Charge amplifier
9 – Laptop with NI 6036 E Data card
10 – IMO drive

Figure 5: Experimental setup

Polytec OFV-302 laser vibrometers are used for acquisition of vibration signals. Class II, Helium Neon lasers emitted by the sensor heads are positioned at a distance of 1 m from the target (an optically smooth surface) developed on a specially designed tool (see figure 6). Bell and Rothberg [13] have shown that a single point laser vibrometer, measuring the velocity of a shaft, is insensitive to its profile, despite the fact that the incident beam can change in axial and radial position on the shaft in any arbitrary fashion. Such immunity to target shape gives this measurement technique a significant advantage over, for example, proximity probe measurements.

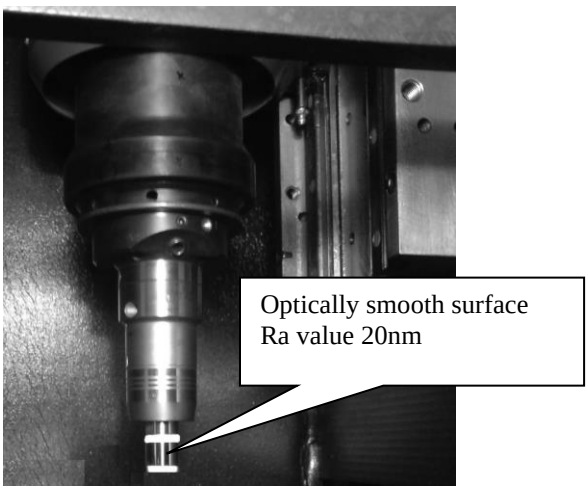

Figure 6 Spindle fitted with optically smooth surface

Rothberg and Halliwell [14] demonstrated how the cross-sensitivity of radial vibrations in the measured velocity. A speckle pattern is a chaotic distribution of light and dark spots formed when coherent light is scattered from a surface, which is comparably rough with respect to the wavelength of light. Rotation of the target surface causes a motion of the speckle pattern, ultimately causing noise in the laser vibrometer output. This noise is repeated with every rotation and contributes energy at the same frequency as the rotational motion and for that reason is referred to as pseudo-vibrations [14]. Even though the researchers working in the field are unable to quantify speckle noise, they have suggested various ways to tackle the problem. Tatar *et. al*.[15] has shown that using an optically smooth surface with 20 nm Ra the problem of speckle noise and cross-sensitivity can be avoided. For this study a specially designed tool (inserted into the collet), representing a target surface, see figure 6 with optically smooth surface was manufactured, the surface roughness was verified using a Talysurf CLI 2000. The safe operating range for the spindle tests are in the range 16000 – 38000 rpm. For this study spindle test runs were performed at speeds of 25,000 rpm.

V. NUMERICAL MODELLING RESULTS

The limit cycle oscillation is obtained by a phase plane plot as shown in Figure 8(a). This is a phase plane plot of radial displacement and velocity, which clearly shows the initial non-steady state and the subsequent steady state behaviour. Since a perfect bearing free of geometrical and topographical defects is assumed here the numerical results shows a single loop in the phase plane plot, which is due to the existence of cage frequency. Since the shaft is assumed to perfectly balanced the effect of shaft frequency does not have a major contribution. Note that a widely spread loaded region also inhibits the variable compliance effect, thus no significant contributions at ball-pass frequency is observed. Figure 8(b) shows the locus of the radial oscillations in X and Y directions. The displacement along the Y direction is 32 µm positive and 48 µm negative, whereas the displacement along the other radial direction X is ± 40 µm. The difference in the oscillations may be attributed to the variable compliance effect [12].

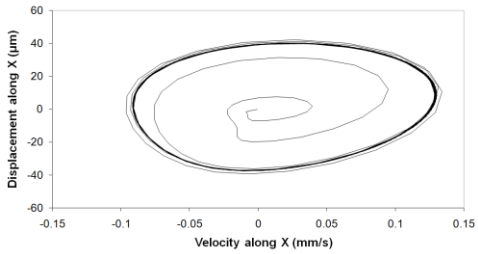

Figure. 8 (a) Numerical – Phase plane plot

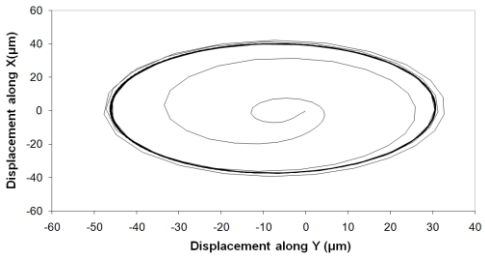

Figure. 8 (b) Numerical – X-Y Locus

Published By:
Blue Eyes Intelligence Engineering
and Sciences Publication (BEIESP)

VI. COMPARISON WITH EXPERIMENTAL SPECTRA

Numerical model for spindle dynamics can be further detailed by including effect of lubrication. Therefore, it is important to numerically predict results which can be compared with the experimental findings. In order to compare the numerical results with the experiments care was taken to use identical conditions. Figure 9(a) shows the FFT spectrum of radial vibrations along X axis and the same for experiment is shown in Figure 9(b). Since the vibration amplitudes other than shaft frequency are relatively small a qualitative comparison is done.

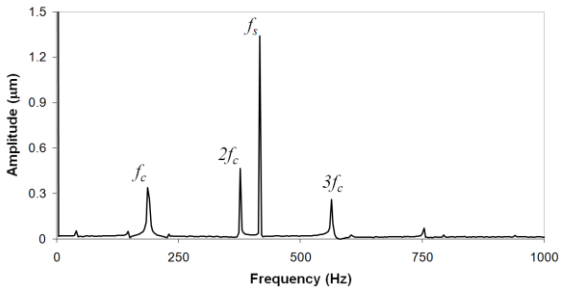

Figure. 9(a). FFT – Numerical

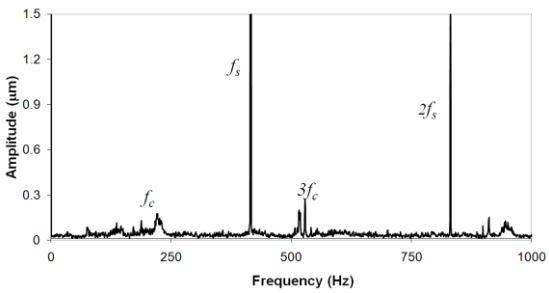

Figure. 9(b). FFT – Experimental

The highest vibration amplitude recorded for numerical is 1.34 µm at 416.7 Hz at the shaft frequency (f_s). Experimentally, the highest vibration amplitude is 11.7 µm, which occurs at 416 Hz, the shaft frequency (f_s). The difference of 10.36 µm may be due to the spindle unbalance in practice. In the numerical model, the eccentricity is considered to be zero. However, a more likely explanation is that the numerical model lacks sources of damping, mainly dry friction in bearing housing, as well as thermo-mechanical distortions. Thus, comparisons are only valid on frequency rather than amplitude contributions (qualitative comparisons). The noticeable peaks occur for cage frequency and its harmonics in both cases. For the numerical model, the cage frequency occurs at 186.6 Hz with vibration amplitude of 0.34 µm. The same for experiment occurs at 188 Hz with amplitude of 0.13 µm. Table 2 below shows the comparison between dominant frequencies in both cases.

Table 2: Frequency and Vibration amplitude comparison

	Numerical		Experiment	
	Frequency (Hz)	Amplitude (µm)	Frequency (Hz)	Amplitude (µm)
f_s	416.7	1.34	416	11.7
f_C	186.6	0.34	188	0.131
$2f_C$	376.6	0.466	370	0.058
$3f_C$	563.3	0.26	554	0.08

The comparison between numerical model and experimental spectra shows good agreement. The load acting on a ball as it goes through a revolution about the shaft obtained is shown in Figure 10. The load acting on a ball at every degree of its procession is obtained. The minimum load was found to be 4.014 N and its maximum at 49 N. This load was given as an input for the lubrication code developed using visual C++ and the contact parameters for one rotation of a ball inside the bearing filled with synthetic poly urea grease are found assuming the contact conditions to be quasi static and no squeeze.

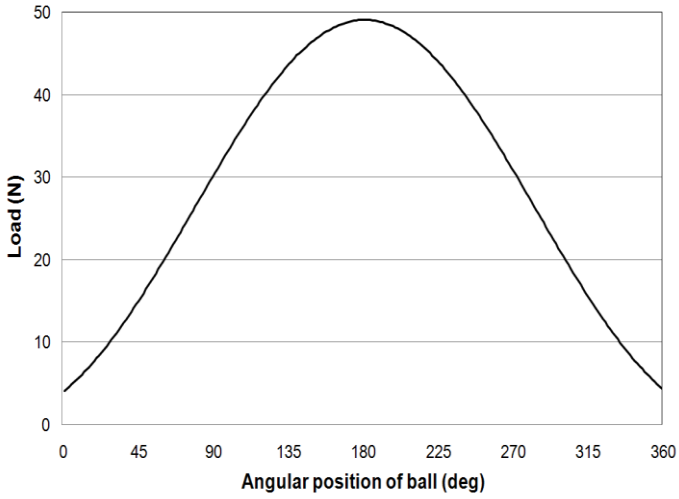

Figure 10: Load per ball

According to the classical Hertzian theory, in an elastostatic contact, the pressure distributions would be ellipsoidal. Hertzian pressures were found to be 2.37, 1.96 and 1.21 GPa for loads of 49, 24 and 4N respectively. Figure 11 shows the pressure, film thickness and plug flow profile for an applied load of 4N. The pressure generated in the contact for this load is found to be 1.12 GPa. Hence the Hertzian contact area is small the EHL spike has influenced the pressure at the centre of the contact. The central and minimum film thickness for a load of 4N are $1.61\ \mu m$ and $1.2\ \mu m$ respectively. Surface profile measurements carried out for balls and races using a Talysurf CLI 2000 gives an average surface roughness value of $0.46242\mu m$. The regime of lubrication can be found using ψ, the ratio of film thickness to the average surface roughness. For conditions in Figure 11, ψ is 2.6, hence the regime of lubrication is in transition between hydrodynamic and full EHL condition. Figure 12 shows the pressure, film thickness and plug flow profile for an applied load of 24N. For this case the central and minimum film thickness observed are $1.64\ \mu m$ and $1.2\ \mu m$ respectively.

Published By:
Blue Eyes Intelligence Engineering
and Sciences Publication (BEIESP)

The ψ value for this operating condition is 2.6. The maximum pressure rise recorded for this contact is $1.93\ GPa$, which is 81% of the maximum Hertzian contact pressure, thus the condition is in transition between hydrodynamic and full EHL condition. The pressures generated, corresponding film thickness and plug flow profile in the contact conjunction for an applied load of 49N is shown in Figure 12. The maximum pressure is $2.32\ GPa$, which is 98 % of the maximum Hertzian pressure. The operating regime is nearly purely EHL as the ψ is 2.9, with a minimum film thickness of $1.33\ \mu m$. Clear demonstration of the pressure profiles in 3D is shown in Figures 17-19

As the lubricant enters the contact, the lubricant viscosity increases dramatically and localised surface deformations make a parallel film thickness Grubin et.al. [16]. This is followed by an equally sharp decline to ambient viscosity levels at the exit of the contact to ensure continuity of flow condition. To compensate for the loss of lubricant viscosity at the contact exit, a constriction is formed close to the exit. A large pressure peak is thus generated next to the constriction on the upstream side, and on the downstream the pressure rapidly declines to less than the dry Hertzian values. It is found that the peak pressure is usually larger than the maximum Hertzian contact pressure and diminishes with lubricant starvation. The exit constriction to the EHL film is found to be curved in order to fit into the contact boundary. This effect is known as the 'horse-shoe' constriction. The horse-shoe effects for applied loads of 4, 24 and 49N are shown in Figures 14-16.

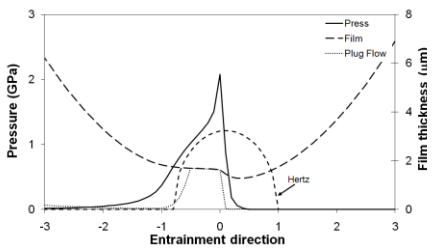

Figure 11: Contact Parameters load 4N

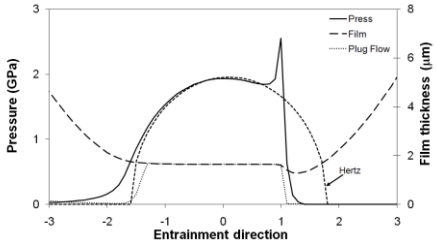

Figure 12: Contact Parameters load 25N

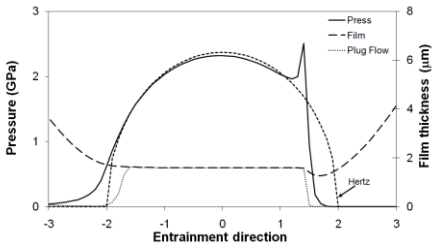

Figure 13: Contact Parameters load 49N

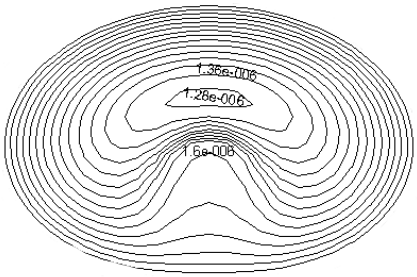

Figure 14: Film Contour load 4N

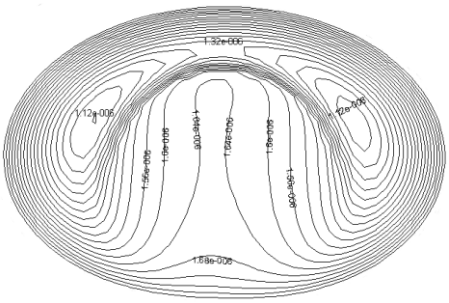

Figure 15: Film Contour load 25N

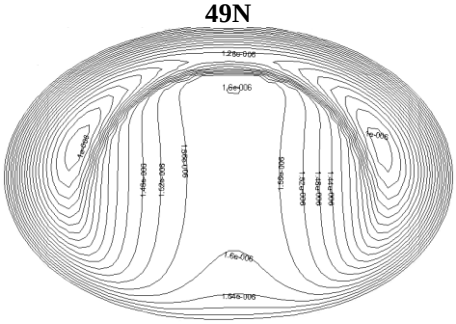

Figure 16: Film Contour load 49N

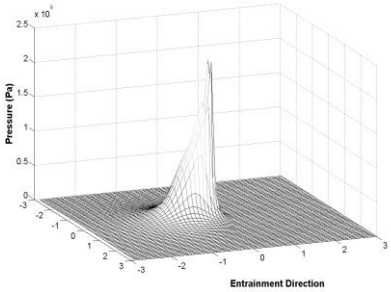

Figure 17: 3D Pressure Profile load 4N

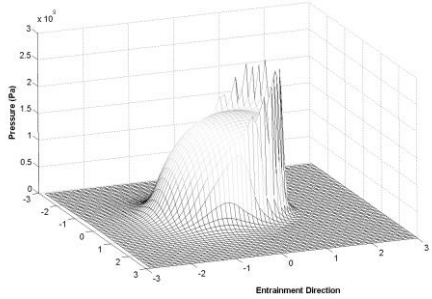

Figure 18: 3D Pressure Profile load 25N

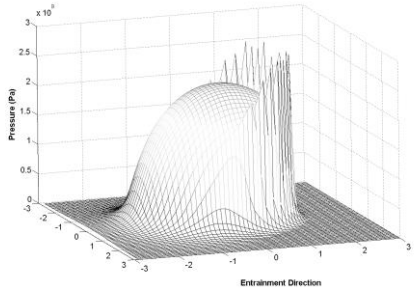

Figure 19: 3D Pressure Profile load 49N

Core formation

As the lubricant enters into the contact area its shear stress increases dramatically due to high generated pressures, which makes the lubricant behave as a solid core which fills the entire contact region, Cann et.al. [17]. The contact, the lubricant can be described as a core in a glassy state, sandwiched between thin shear zones, probably of molecular proportions, in which the difference in velocity of the solidified core relative to the mean entraining velocity is accommodated. The Herschel Bulkley flow equation is considered for this study assuming that grease behaves as Bingham solid, thus:

$$\tau = \tau_0 + \phi |D|^n \qquad (8)$$

which infers that grease behaves as a solid if the applied shear stress is below the yield shear stress (τ_0). This value varies from 3.5 to 1000 Pa. for mineral oils as the base oil according to Kauzlarich and Greenwood [18]. For this study the initial value for yield shear stress was assumed to be 100 Pa.

Published By:
Blue Eyes Intelligence Engineering
and Sciences Publication (BEIESP)

VII. CONCLUSION

An attempt to describe the bearings behaviour is made by using a numerical model with five degrees of freedom. Comparison of the numerical results with experiments results shows a very close match. The small differences between the results may be attributed to the effect of damping, frictional drag of lubricant and inertial effects of the support structure. The interactions between cage with races and cage to balls also contribute to the differences. Pressure, film thickness and plug flow for grease lubricated contacts for different loads are also shown.

NOMENCLATURE

A - Distance between raceway groove curvature

f_C - Cage frequency

D - Ball diameter

f_s - Shaft Frequency

F_x, F_y, F_z - Force acting on corresponding axis

I_{xx}, I_{yy}, I_{zz} -MI of inertia in corresponding axis

K - load-deflection constt of prop for all ball cont

L - Distance from spindle centre to bearing

M - Mass of spindle

n - Number of balls

p_d - Diametrical clearance

P_r - Preload

r - radius

U_x, U_y - Velocities in orthogonal direction

W_i - Load on i^{th} ball

W_0 - Initial load

$W_{x_0}, W_{y_0}, W_{z_0}$ - Initial load acting on corresponding axis

x_b, y_b - Ball displacements in X and Y axis

x, y, z - Displacement in corresponding axis

z_0 - Initial axial deflection

α_0 - Free/Initial Contact angle

α_p - Preloaded contact angle

δ_0 -Initial deflection

θ_i - Angular position of ith rolling element

ϕ, φ - Tilts about the X and Y

ω_c - Angular velocity cage

ω_i - Angular velocity inner race

ω_o - Angular velocity outer race

REFERENCES

1) Rahnejat, H. and Gohar, R, 'The vibrations of radial ball bearings', Proc. Instn Mech. Engrs, Part C, J. Mechanical Engineering Science, 1985, 199(C3), 181–193.
2) Wardle, F. P. and Poon, S. Y, 'Rolling Bearing Noise-Cause and Cure', July–August 1983 (CME).
3) Matsubara M, Rahnejat, H. and Gohar, R, 'Computational modelling of precision spindles supported by ball bearings', Int. J. Mach. Tools Manufacture., 1988, 28(4), 429–442.
4) Aini, R., Rahnejat, H. and Gohar, R. 'A five degrees of freedom analysis of vibrations in precision spindles', Int. J. Mach. Tools Manufacture, 1990, 30(1), 1–18.
5) Aini, R. 'Vibration monitoring and modelling of shaft/bearing assemblies under concentrated elastohydrodynamic conditions', PhD thesis, Kingston University, January 1990.
8) Aini, R., Rahnejat, H. and Gohar, R, 'Vibration modelling of precision spindles supported by lubricated bearings', Trans. ASME, J. Tribology, April Vol. 124, 2002 158-165.
9) H. Hertz, Gesammelte Werke, Vol.1, 1995. (H. Hertz, Miscellaneous Papers, trans. D.E. Jones, G.A. Schott, Macmillan, London, 1896).
11) Rahnejat H, 'Computational modelling of problems in contact dynamics', Engineering analysis, 2:44, 1985, 192-197.
12) N. Lynagh, H. Rahnejat, M. Ebrahimi and R. Aini, 'Bearing induced vibration in precision high speed routing spindles', Int. J. Mach. Tools Manufacture, Volume 40, Issue 4, March 2000, Pages 561-577.
13) J. R. Bell and S. J. Rothberg, 'Laser vibrometers and contacting transducers, target rotation and 6 degree-of-freedom vibration: what do we really measure?', Journal of Sound and Vibration, 237 (2000), 245-261.
14) S. J. Rothberg and N. A. Halliwell, 'On the use of laser vibrometry for rotating machinery measurements', Proceedings of IMechE, 25th International Conference on Vibrations in Rotating Machinery, Bath, (1992), 409-415.
15) Kourosh Tatar, Matti Rantatalo and Per Gren, 'Laser vibrometry measurements of an optically smooth rotating spindle', Mechanical Systems and Signal Processing, Volume 21, 4,(2007) 1739-1745.
16) Grubin, A.N., Vinogradaova, I.E., and Ketnva, F., eds, 'Investigation of the contact machine components', Central Sci. Res. Inst. Tech. Mech. Eng., Book 30, (D.S.I.R. translation 337), Moscow, 1949.
17) Cann, P. M., Williamson, B. P., Coy, R. C. and Spikes, H. A., 'The behaviour of greases in elastohydrodynamic contacts', Appl. Phys. A, 25 (1992), 124-132.
18) Greenwood, J. A. and Kauzlarich, J. J, "Inlet shear heating in elastohydrodynamic lubrication", Trans. ASME, J. Lubric. Technol, 95(1973), 417–426.

Published By:
Blue Eyes Intelligence Engineering
and Sciences Publication (BEIESP)